Fluid/thermal/chemical non-equilibrium simulation of hypersonic reentry vehicles

Subramani Sockalingam[1] and Ala Tabiei[2]
Department of Aerospace Engineering & Engineering Mechanics
University of Cincinnati, Cincinnati, OH 45221-0070

ABSTRACT

A multi-physics frame work has been setup for the simulation of surface heat flux for nonablating hypersonic reentry vehicles and presented in this paper. The main goal of this work was to set up a simple approach for the heat flux prediction during the reentry of the vehicle. The vehicle considered in the calculation is an axisymmetric vehicle flying at zero degree angle of attack. Chemical nonequilibrium in the flowfield is simulated by implementing a set of finite rate equations in the laminar finite rate model in FLUENT. The frame work set up was validated with the results available in the literature. Good correlation was observed between the results from the commercial code with the implemented equations and the results from the literature.

1. INTRODUCTION

The hypersonic reentry vehicle is immersed in a hot gas as the kinetic energy of the flow is dissipated by viscous effects. The detached shock wave in front of the vehicle also increases the gas temperature. Thermal Protection System (TPS) is used to insulate the hypersonic reentry vehicle from the high temperature during the reentry [1]. Numerical simulation of the heat transfer during the reentry flight and the material thermal response of the TPS can be challenging due to the multiphysics interactions like chemically reacting flow, radiation and heat conduction. A literature survey was conducted to examine the fluid thermal coupling procedures for hypersonic reentry vehicles. It was identified that aero thermal heat flux prediction and material thermal response is evaluated using in house codes like SACCARA (Sandia Advanced Code for Compressible Aerothermodynamics Research and Analysis) [2], GIANTS (Gauss-Siedel Implicit Aerothermodynamic Navier-Stokes code with thermo chemical surface conditions) [3], COYOTE II [2], FIAT (Fully Implicit Ablation and Thermal response code) [3] and so on. With the advances in commercial Computational Fluid Dynamics (CFD) and Finite Element Analysis (FEA) codes, the prediction of aero thermal heat flux and the material thermal response of the TPS using these codes are highly feasible. The primary issue of this work is to identify and understand the capability of these codes for predicting the chemically reacting hypersonic flow. FLUENT is used as the CFD code as it is capable of modeling the species transport apart from the basic fluid flow [4]. The chemically reacting hypersonic flow for an axisymmetric vehicle at zero degree angle of attack is solved using FLUENT and in the current work.

---

[1]Graduate Research Assistant

[2]Associate Professor, ala.tabiei@uc.edu

2. METHODOLOGY AND GOVERNING EQUATIONS

2.1. GOVERNING CFD EQUATIONS

The computational fluid dynamics calculations are performed using the numerical code FLUENT. The fluid has been modeled as a reacting gas in thermal equilibrium and chemical non-equilibrium. The flow is assumed to be laminar. The governing equations are as follows:

Continuity equation

$$\frac{\partial \rho}{\partial t} + \nabla \cdot (\rho V) = 0 \tag{1}$$

Species equation

$$\frac{\partial (\rho m_i)}{\partial t} + \nabla \cdot (\rho V m_i) + \nabla \cdot J_i = R_i \tag{2}$$

Momentum equation

$$\frac{\partial (\rho V)}{\partial t} + \nabla \cdot (\rho V V) + \nabla p = \nabla \cdot \overline{\overline{\tau}} \tag{3}$$

Where

$$\overline{\overline{\tau}} = \mu \left[(\nabla V + \nabla V^T) - \frac{2}{3} \nabla \cdot V I \right] \tag{4}$$

Energy equation

$$\frac{\partial (\rho E)}{\partial t} + \nabla \cdot (V(\rho E + p)) = \nabla \cdot \left[\lambda \nabla T - \sum_i h_i J_i + (\overline{\overline{\tau}} \cdot V) \right] \tag{5}$$

Where

$$E = h - \frac{p}{\rho} + \frac{v^2}{2} \tag{6}$$

$$h = \sum_j m_j h_j \; h_j = \int_{T_{ref}}^{T} c_{p,j} dT \tag{7}$$

The ideal gas equation of state is used

$$p_i = \rho_i R_i T \tag{8}$$

$$p = \sum_i p_i \tag{9}$$

2.2. CHEMICAL NON-EQUILIBRIUM MODEL

As mentioned earlier the fluid which is air surrounding the reentry vehicle is at a high temperature due to kinetic energy dissipation and shock wave. The high temperature causes air to dissociate and even ionize. The temperature in the nose area of Apollo reentry was about 11,000 K at a Mach number of 35 [5]. The constant specific heat assumption becomes invalid at those temperatures. Chemical nonequilibrium assumption says that the characteristic chemical reaction time is the same as the characteristic time of fluid motion. The laminar finite-rate model in FLUENT computes the chemical species production rate using modified Arrhenius equation. The net source term of chemical species *i* is computed as [4]

$$R_i = M_i \sum_{R=1}^{N_R} \hat{R}_{i,r} \tag{10}$$

The net rate of creation of species *i* in reaction *r* is given by

$$\hat{R}_{i,r} = \Gamma(\nu''_{i,r} - \nu'_{i,r}) \left[k_{f,r} \prod_{j=1}^{N} \left[C_{j,r} \right]^{\nu'_{j,r}} - k_{b,r} \prod_{j=1}^{N} \left[C_{j,r} \right]^{\nu''_{j,r}} \right] \tag{11}$$

The forward rate constant for reaction *r* is modeled using the Arrhenius expression

$$k_{f,r} = A_r T^{\beta_r} \exp[-(E_r / RT)] \tag{12}$$

The backward rate constant for reaction *r* is computed from the forward rate using

$$k_{b,r} = \frac{k_{f,r}}{K_r} \tag{13}$$

The two-temperature model of Park [2] consisting of five species (N_2, O_2, NO, N, O) is used. The Park model uses the average of translational and vibrational temperatures to calculate the rate constants [5]. The reaction rate coefficients and the characteristic temperature of dissociation are given in Table 1. In [2] the Park model is used with the assumption of thermo-chemical nonequilibrium whereas in this work it is used with the assumption of thermal equilibrium and therefore it is assumed that all the internal energy modes are in equilibrium at temperature T.

2.3. TRANSPORT PROPERTIES

The transport properties of the species are obtained from the kinetic theory of gases [4]. The fluid viscosity is defined using kinetic theory as

$$\mu_i = \frac{2.67.10^{-6} \sqrt{M_i T}}{\sigma_i^{\,2} \Omega_{\mu i}} \tag{14}$$

The Lennard-Jones parameters used were obtained from ref [5] and [6] and are given in Table 2.

The thermal conductivity of a pure gas is defined using kinetic theory as

$$\lambda_i = \frac{15}{4}\frac{R}{M_i}\mu\left[\frac{4}{15}\frac{C_{pi}M_i}{R}+\frac{1}{3}\right] \tag{15}$$

The mass diffusion coefficient is defined using kinetic theory as

$$D_{ij} = 0.00188\frac{\left[T^3\left(\frac{1}{M_i}+\frac{1}{M_j}\right)\right]^{1/2}}{p\sigma_{ij}{}^2\Omega_{Dij}} \tag{16}$$

The mass diffusion coefficient of species *i* in the mixture is defined as

$$D_{im} = \frac{1-X_i}{\sum_j (X_j / D_{ij})} \tag{17}$$

The mixture values of μ and k for the chemically reacting gas is defined using Wilke's rule [4]

$$\mu = \sum_i \frac{X_i\mu_i}{\sum_j X_j\phi_{ij}} \tag{18}$$

$$\lambda = \sum_i \frac{X_i\lambda_i}{\sum_j X_j\phi_{ij}} \tag{19}$$

Where

$$\phi_{ij} = \frac{1}{\sqrt{8}}\left(1+\frac{M_i}{M_j}\right)^{-1/2}\left[1+\left(\frac{\mu_i}{\mu_j}\right)^{1/2}\left(\frac{M_j}{M_i}\right)^{1/4}\right]^2 \tag{20}$$

2.3. THERMAL EQUILIBRIUM MODEL

When the fluid temperature increases the internal energy modes get excited and the specific heat ratio is not constant. Thermodynamic properties of high temperature air in the form of polynomial curve fits exist which can used to implement this model. This model assumes that the thermal relaxation time is much smaller than characteristic time of fluid motion.

The values of specific heat of all the species are required for the case of thermal equilibrium. The curve fits provided in [7] are used. Originally they are curve fit with the following polynomial with five ranges 300 K ≤ T ≤ 1000 K, 1000 K ≤ T ≤ 6000 K, 6000 K ≤ T ≤ 15000 K, 15000 K ≤ T ≤ 25000 K, 25000 K ≤ T ≤ 30000 K

$$C_{pi} = A_1 + A_2T + A_3T^2 + A_4T^3 + A_5T^4 \tag{21}$$

Since FLUENT allows only three ranges for the temperature dependent specific heat and also because of the limitation that specific heat values cannot be modified in FLUENT [4],

Table 1 Reaction rate constants $M_{vib} = N_2, O_2, NO$ $M_{atom} = N, O$

Reaction		M	Ar	b	Er/R
1	$N_2 + M \Leftrightarrow N + N + M$	M_{nib}	7.0E+18	−1.6	113200
		M_{atom}	3.0E+19	−1.6	113200
2	$O_2 + M \Leftrightarrow O + O + M$	M_{vib}	2.0E+18	−1.5	59500
		M_{atom}	1.0E+19	−1.5	59500
3	$NO + M \Leftrightarrow N + O + M$	M_{vib}	5.0E+12	0.0	75500
4	$N_2 + O \Leftrightarrow NO + N$	–	6.4E+14	−1.0	38400
5	$NO + O \Leftrightarrow O_2 + N$	–	8.4E+09	0.0	19450

Table 2 Lennard-Jones parameters

Species	σ, °A	ε / k_1, K
N_2	3.681	91.5
O_2	3.433	113
NO	3.470	119
N	3.298	71.4
O	3.05	106.7

the first and second ranges and the fourth and fifth ranges are combined and curve fit with seventh degree polynomials. The specific heat of the mixture is calculated as a mass fraction average of the pure species heat capacities [4]

$$c_p = \sum_j m_j c_{p,\,j} \tag{22}$$

2.4. BOUNDARY CONDITIONS

Pressure far-field conditions are used in FLUENT to model a free-stream condition at infinity, with free-stream Mach number and static conditions being specified [4]. The freestream conditions for the calculations are given in Table 3 [2]. The free stream static pressure, Mach number and static temperature are given as input to the pressure far-field.

Wall boundary condition is used to bind the solid and fluid region in FLUENT [4]. For non-ablating case, a no-slip condition is used. It indicates that the fluid sticks to the wall. An isothermal wall is used for the thermal boundary condition. A constant wall temperature of 294.4 K was assumed for the initial simulation. Fully catalytic wall with species concentrations equal to the freestream composition (77% N_2 and 23% O_2 by weight) is assumed. The Axis boundary condition is specified at the centerline of the axisymmetric geometry.

2.5. NUMERICAL TECHNIQUE

The density-based solver in FLUENT solves the governing equations of continuity, momentum, energy and species transport simultaneously [4]. The system of governing equations solved by the FLUENT solver in vector form is given by [4]

Figure 1 IRV-2 War head.

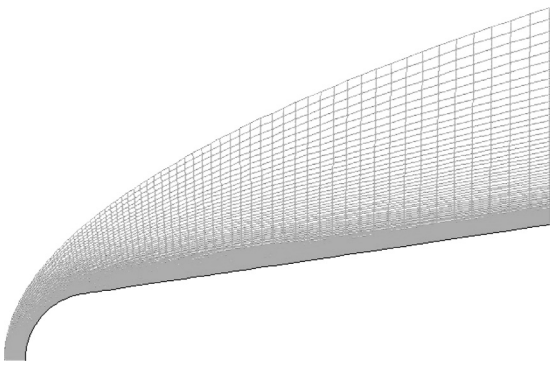

Figure 2 Computational domain used in the CFD.

$$\frac{\partial}{\partial t}\int_V WdV + \int [F - G] \bullet \, dA = \int_V HdV \tag{23}$$

The inviscid flux vector F in Eqn 23 is computed using a flux-vector splitting scheme Advection Upstream Splitting Method (AUSM) [4]. The spatial discretization is specified using a second order upwind scheme. Time discretization is accomplished using an implicit method.

Table 3 Freestream conditions

Traj. Point	Time (sec)	Altitude (m)	Velocity (m/s)	Temp. (K)	Pressure (Pa)	Mach No.
1	0	66935	6780.6	227.81	8.1757	22.41
2	4.25	55842	6788.3	258.02	37.362	21.08
3	6.75	49290	6785.2	270.65	88.118	20.58
4	8.75	44042	6773.0	261.40	169.50	20.90
5	10.25	40108	6752.4	250.35	287.14	21.29
6	11.50	36836	6722.0	241.50	445.52	21.59
7	12.50	34229	6684.3	234.30	644.52	21.79
8	13.25	32283	6644.9	228.76	863.14	21.92
9	13.95	30480	6596.7	226.91	1127.6	21.85
10	14.75	28444	6429.6	224.92	1521.6	21.39
11	16.00	25386	6077.2	221.95	2398.0	20.35
12	17.25	22523	5605.4	219.07	3745.5	18.89
13	18.00	20923	5268.0	217.48	4803.3	17.82
14	18.75	19424	4900.9	216.65	6074.4	16.61
15	19.25	18485	4646.6	216.65	6994.8	15.75
16	20.00	17167	4262.1	216.65	8576.4	14.45
17	20.75	15959	3885.5	216.65	10352	13.17
18	21.67	14616	3445.2	216.65	12896	11.68
19	22.75	13239	2980.3	216.65	16066	10.10
20	24.00	11855	2542.5	216.65	19706	8.62
21	24.75	11118	2317.7	216.65	22278	7.86
22	25.25	10661	2180.4	219.04	23975	7.35
23	26.50	9623	1876.1	225.84	28157	6.23
24	33.50	5795	822.9	250.48	48524	2.59
25	62.05	0	186.3	288.15	101325	0.55

3. RESULTS AND DISCUSSION

3.1. COMPUTATIONAL DOMAIN

An axisymmetric IRV-2 vehicle [2] at zero degree angle of attack is considered for the simulations (see Figure 1). The vehicle, which is a sphere-biconic-cylinder, has a nose radius of 0.01905 m and a total length of 1.3866 m. The biconic angles are 8.42° and 6.10° with a break at 0.1488m. The flow field grid for the CFD simulation is a structured grid created using Gridgen [8] and is shown in Figure 2. The first cell spacing near the wall is chosen as 1×10^{-6}m. Figure 3 shows the surface heat flux evaluated by FLUENT for the trajectory point 1 in Table 3. The surface heat flux is plotted versus the y-coordinate which corresponds to the radial direction. The stagnation point heat flux is 601.99415 W/cm^2 for the grid size 64×64 cells in axial and radial directions. The grid was refined to 128×128 to study the effect on the convective heat transfer. The stagnation point heat flux value did not change appreciably compared to the coarser 64×64 grid which is illustrated in figure 3. Two cases are considered for the species at the wall:

Non catalytic wall

In this case the mass fraction gradients at the wall are assumed to be zero [9] which translates to no reactions at the wall that is,

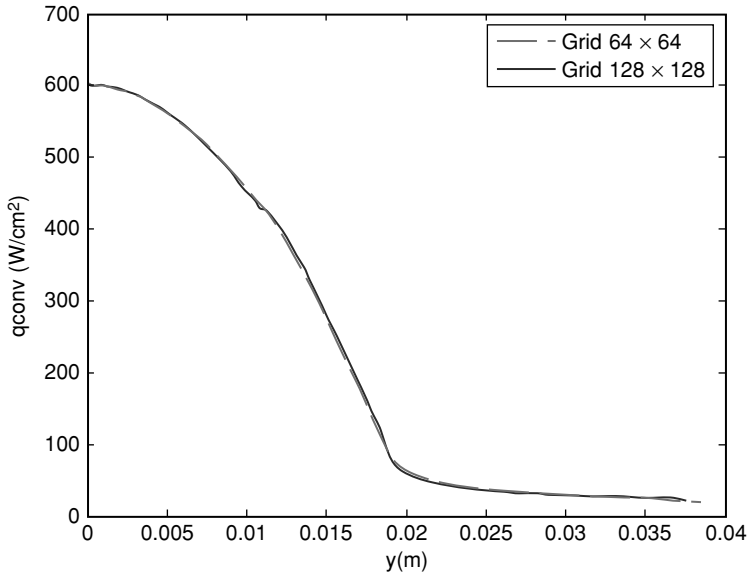

Figure 3 Grid refinement study for surface heat flux.

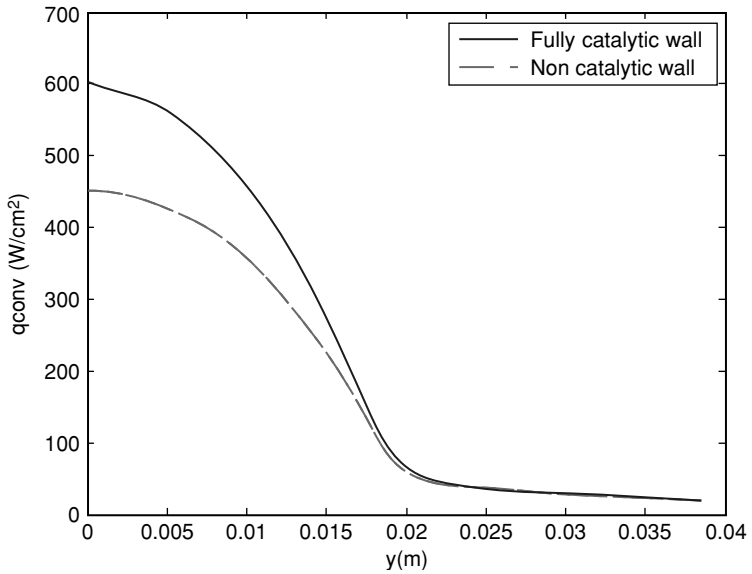

Figure 4 Total surface heat fluxes for fully catalytic and non catalytic wall.

$$\nabla m_i = 0 \tag{24}$$

Fully catalytic wall

In this case all the dissociated atoms are recombined at the wall. The wall material, i.e., the TPS material, in this case, catalyzes chemical reactions at the surface [5]. The species concentration at the surface is assumed to be of freestream composition

$$(m_i)_w = m_{i\infty} \tag{25}$$

Figure 4 compares the surface heat flux in the two cases. The stagnation point heat flux in the first case is 452.32 W/cm^2 whereas in the second case it is 601.99415 W/cm^2 due to the recombination of dissociated species which is an exothermic reaction. It is observed that the stagnation point heat flux in the case of non catalytic wall is about 25% less than that of the flux determined for fully catalytic wall. The contours of static temperature and pressure for the first trajectory point are shown in figures 5 and 6. The surface heat flux distributions for the first three trajectory points are shown in figure 7 and the respective heat flux distributions are shown in figure 8. After the third trajectory point it became difficult to determine the CFD solution using second order numerical scheme with the grid 128×128. Nevertheless using first order numerical scheme enabled to achieve a solution with a compromise in the accuracy. At this time, the CFD mesh is refined further and being investigated with second order scheme and hence the solution is not presented for further trajectory points.

3.2. VALIDATION

Figure 9 compares the total surface heat flux determined using the present method with the heat flux obtained from [2] where the authors performed the computational fluid dynamics calculations using SACCARA (Sandia Advanced Code for Compressible Aerothermodynamics Research and Analysis). The authors have assumed the flow to be in thermo-chemical nonequilibrium. The heat flux data in the form of graph from [2] is extracted using xy Extract, software which extracts data from a graphic contained in a bitmap file.

Three different diffusion models were implemented in the CFD code, they were:

1. Constant Lewis Number = 1.4 [10]
   Lewis number is the ratio of thermal diffusivity to mass diffusivity [11]

$$D_{im} = \frac{\lambda}{L\rho C_p} \tag{26}$$

2. Constant Schmidt Number = 0.5 [2]
   Schmidt number is the ratio between momentum diffusivity and mass diffusivity [11]

$$D_{im} = \frac{\mu}{\rho Sc} \tag{27}$$

3. Maxwell-Stefan Equations
   The multicomponent diffusion coefficient D_{im} is arrived by simplifying the Maxwell-Stefan equations [20]

$$D_{im} = \frac{1 - X_i}{\sum_j (X_j / D_{ij})} \tag{28}$$

The multicomponent diffusion model is computationally expensive as it involves the calculation of binary mass diffusion coefficient. The influence of the different diffusion models on the surface heat flux is shown in Figure 10. The one with constant Schmidt number is found to be a good approximation to the exact diffusion model.

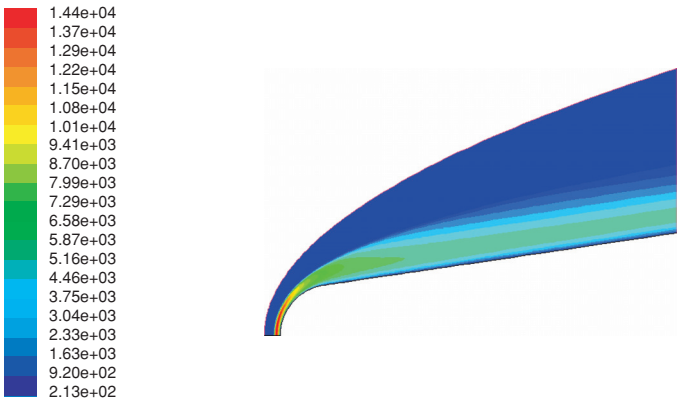

Figure 5 Contours of static temperature for trajectory point 1.

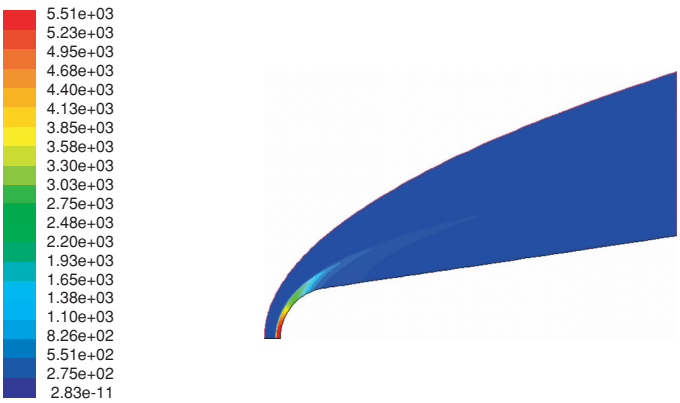

Figure 6 Contours of static pressure for trajectory Point 1.

4.4. VALIDATION OF CONTINUUM ASSUMPTION

One of the aspects of hypersonic flow is the low density at the reentry conditions. Typically the densities at the reentry conditions are very small and hence the mean free path which is the average distance between molecular collisions is comparable to the characteristic length. Therefore the flowfield cannot be considered as continuum and hence the Navier-Stokes equations become non applicable. A non dimensional number called Knudsen number Kn is used to determine the nature of the fluid and it is defined as [12]

$$Kn = \frac{\lambda}{L} \tag{29}$$

where λ the mean free path and L is the characteristic flow field dimension. The mean free path is calculated from kinetic theory using [5]

$$\lambda = \frac{kT}{\sqrt{2}\pi d^2 p} \tag{30}$$

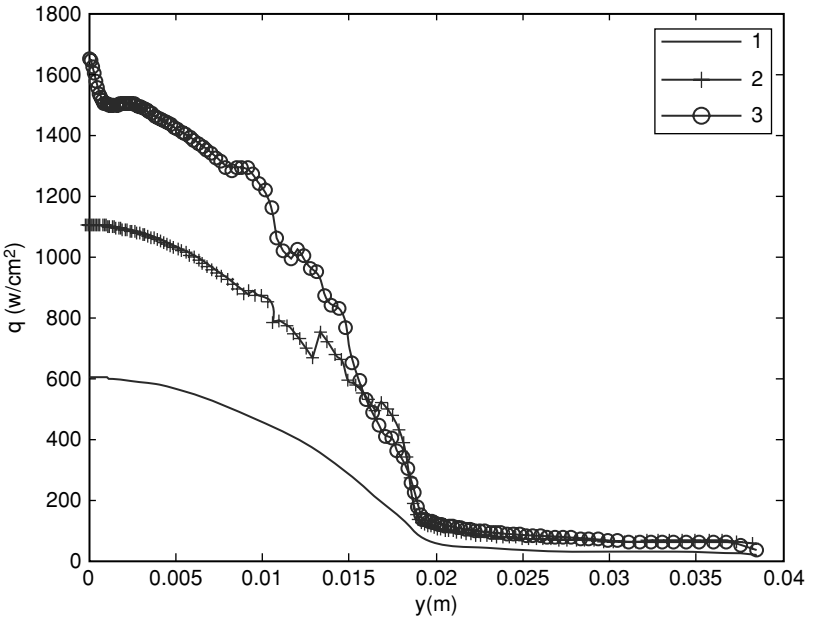

Figure 7 Surface Heat Flux Distributions.

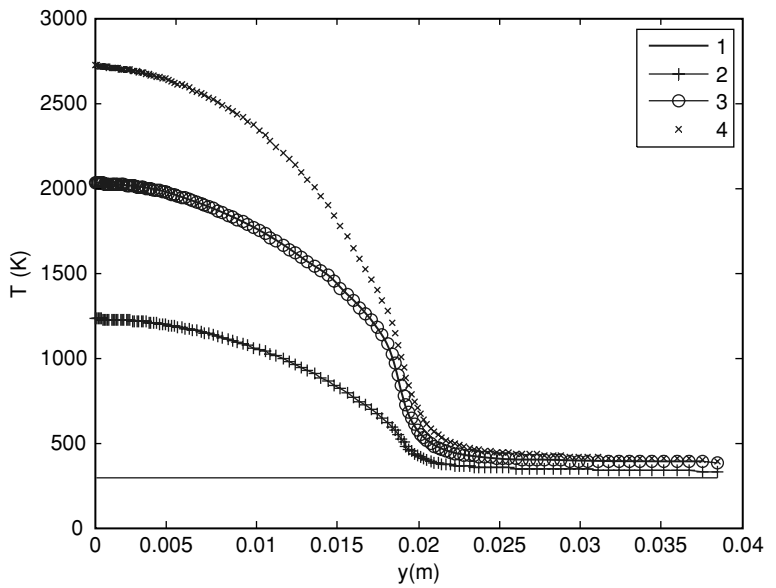

Figure 8 Surface temperature distributions.

where k is the Boltzmann constant which is equal to 1.38×10^{-23} J/K and πd^2 is called collision cross section. The mean free path for the reentry conditions of IRV-2 vehicle is calculated with the characteristic molecular diameter of air as 3.711×10^{-10} m [6] $\lambda = 6.2846e - 4$ m. The Knudsen number for the reentry conditions of IRV-2 vehicle is calculated with the characteristic

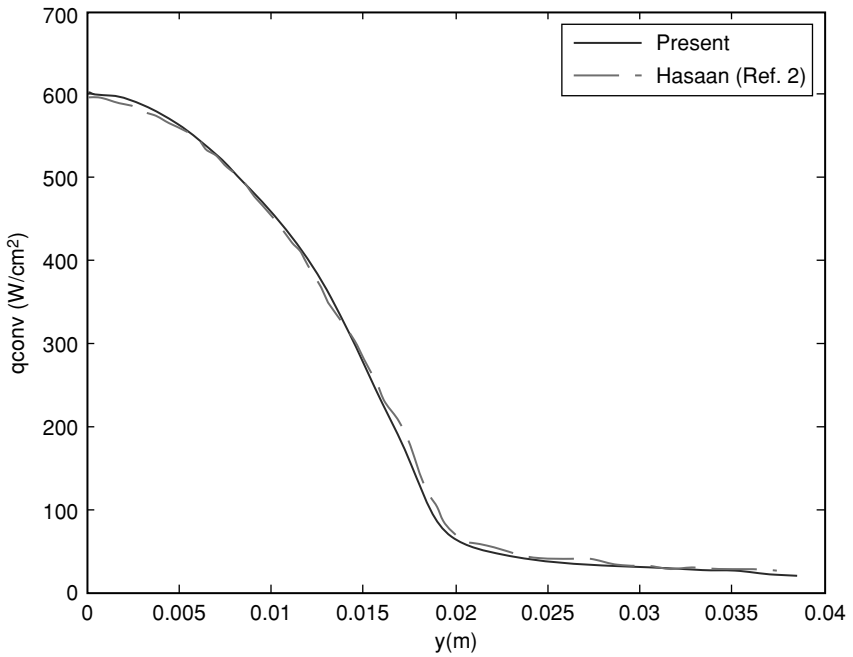

Figure 9 Total surface heat fluxes for fully catalytic wall comparison with Hassan et al [2].

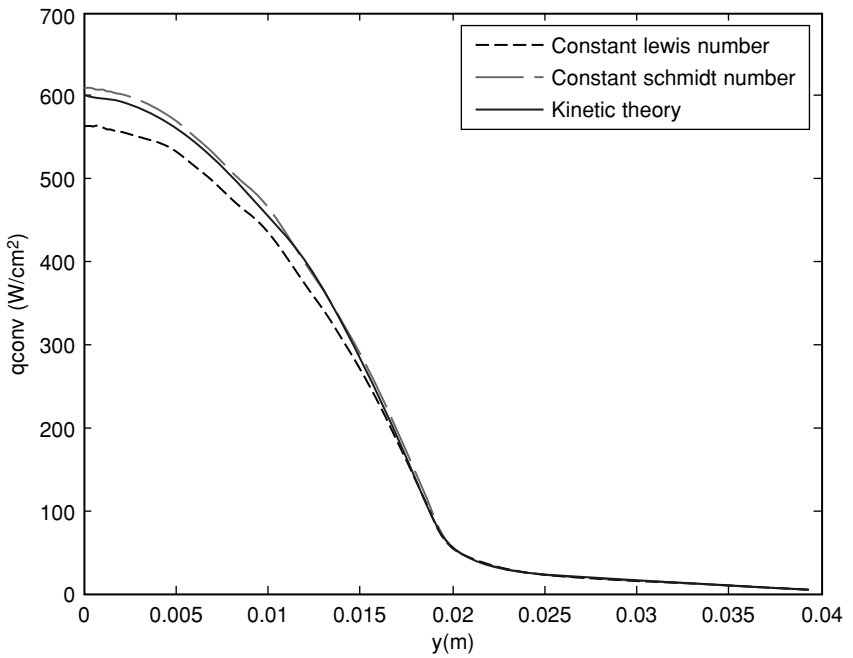

Figure 10 Effect of diffusion model on convective heat transfer rate.

length as the length of the fore body which is 0.1488 m and the Kn is obtained as Kn = 0.0042. The continuum flow assumption is validated with a Knudsen number $Kn << 1$.

5. CONCLUSION

Surface heat flux simulation for nonablating hypersonic reentry vehicles using commercial CFD code FLUENT has been presented. The established procedure was validated with the IRV-2 reentry vehicle and the results were presented. Different diffusion models were implemented into the code and its respective influence on the predicted surface heat flux was presented. The computational difficulties demanded very fine mesh and hence the solution was obtained only for the first three trajectory points of the IRV-2 vehicle. Implementation of fluid/thermal/structural coupling procedure for nonablating and ablating hypersonic reentry vehicles is currently being studied and will be presented at a later paper.

ACKNOWLEDGMENT

The authors thank Ohio Super Computer Center for the computing support.

REFERENCES

[1] Laub, B., Venkatapathy, E., "Thermal Protection System Technology and Facility Needs for Future Planetary Missions," *International Workshop on Planetary Probe Atmospheric Entry and Descent Trajectory Analysis and Science, 2003*.

[2] Hassan, B., Kuntz, D. W., and Potter, D. L., "Coupled Fluid/Thermal Prediction of Ablating Hypersonic Vehicles," *AIAA Paper No. 98-0168, Jan 1998*.

[3] Olynick, D., Chen, Y. K., "Forebody TPS sizing with Radiation and Ablation for the Stardust Sample Return Capsule," AIAA *Paper No. 97-2474, 1997*.

[4] FLUENT 6.3 Documentation, FLUENT Inc., 2006.

[5] Anderson, J.D., Jr., "*Hypersonic and High Temperature Gas Dynamics*," McGraw-Hill, New York, 1989.

[6] Svelha, R. A., "Estimated Viscosities and Thermal Conductivities of Gases at High Temperatures," *NASA TR R-132, 1962*.

[7] Gupta, R. N., Yos, M., Thompson, R. A., "A Review of Reaction Rates and Thermodynamic and Transport Properties for the 11-Species Air Model for Chemical and Thermal Non-equilibrium Calculations to 30000 K," *NASA TM-101528, 1989*.

[8] Gridgen user's Manual, Pointwise Inc., 2006.

[9] Gupta, R. N., "Aerothermodynamic Analysis of Stardust Sample Return Capsule with Coupled Radiation and Ablation," *Journal of Spacecraft and Rockets, Vol.37, No.4, July–August 2000*.

[10] Desmeuzes, C., Duffa, G., and Dubroca, B., "Different Levels of Modeling for Diffusion Phenomena in Neutral and Ionized Mixtures," *Journal of Thermophysics and Heat Transfer, Vol. 11, No.1, January–March 1997*.

[11] Serrancanta, R. C., "*Development of Numerical Codes for the Evaluation of Combustion Processes. Detailed Numerical Simulations of Laminar Flames," September 2002*.

[12] Regan, F. J., Anandakrishnan, S. M., "*Dynamics of Atmospheric Re-entry*," American Institute of Aeronautics and Astronautics, 1993.

NOMENCLATURE

A_n coefficients of polynomial curve fits for thermodynamic properties
n = 1, 2 … 5

A_r, β_r, E_r	constants in the Arrhenius expression of the rate constant
C_{pi}	specific heat of species *i*, J/kg.K
C_p	specific heat of the mixture, J/kg·K
C_H	convective heat transfer coefficient, W/m^2 K
C_i	molar concentration of species of *i*, kgmol/m^3
D_{ij}	binary mass diffusion coefficient of species *i* in species *j*, m2/s
D_{im}	mass diffusion coefficient of species *i* in the mixture, m2/s
E	specific total energy, J/kg
E_r	activation energy, J/kgmol
F	inviscid flux vector
G	viscous flux vector
h	enthalpy, J/kg
H	source terms vector
J_i	mass diffusion flux of species *i*, kg/m^2 s
k_f	forward reaction rate, cm^3/mol s
k_b	backward reaction rate, cm^3/mol s
Kn	Knudsen number
L	Lewis number = 1.4
m_i	mass fraction of species *i*
M_i	molecular weight of species *i*, kg/kg mol
p_i	partial pressure, Pa
q	heat transfer rate, W/m^2
p	pressure, Pa
R	universal gas constant, 8314 J/kgmol K
R_i	net rate of production of species *i*, kg/m^3 s
$\hat{R}_i,r$	reaction rate of species *i* in reaction *r*, kgmol/ m^3 s
Sc	Schmidt number = 0.5
T	temperature, K
V	velocity vector
W	vector of CFD unknowns
X_i	mole fraction of species *i*
ρ	density, kg/m^3
μ	viscosity, kg/ms
$\bar{\bar{\tau}}$	stress tensor
σ_i	characteristic molecular diameter of species *i*, m
Ω	collision integrals
υ	stoichiometric coefficients
λ	thermal conductivity, W/mK
σ	Stefan-Boltzmann constant, 5.6697×10^{-8} J/m^2 K^4 s

Subscripts

aw	adiabatic wall
cond	conduction
f	fluid
w	wall
rad	radiation
stag	stagnation property
∞	free stream